Inorganic Chemistry

Article

pubs.acs.org/IC

Flexible and Dynamic Thermal Behavior of Self-Catenated $[\{Ni_3(H_2O)_3(Bpa)_4\}(V_6O_{18})]\cdot 8H_2O$ Constructed from 10-c Heterometallic Inorganic−Organic Clusters

Roberto Fernández de Luis,[†] José L. Mesa,[‡] M. Karmele Urtiaga,[†] Edurne S. Larrea,[†] Teófilo Rojo,[‡] and María I. Arriortua*[,†]

[†]Departamento de Mineralogía y Petrología and [‡]Departamento de Química Inorgánica, Facultad de Ciencia y Tecnología, Universidad del País Vasco/EHU, Apdo. 644, E-48080 Bilbao, Spain

Supporting Information

ABSTRACT: The hydrothermal treatment of $Ni(NO_3)_2\cdot 6H_2O$, $NaVO_3$, and Bpa (1,2-Di(pyridyl)ethane) ($C_{12}H_{12}N_2$) at 120 °C during 3 days leads to green single crystals of the title compound. The single crystal X-ray diffraction reveals that $[\{Ni_3(H_2O)_3(Bpa)_4\}(V_6O_{18})]\cdot 8H_2O$ crystallizes in the monoclinic system, $P2_1/c$ space group, with a = 13.5536 (2), b = 19.0463 (2), c = 27.7435 (3) Å, β = 112.3880 (10)°, V = 6622(3) Å^3, with R1(obs) = 0.0558, wR2(obs) = 0.1359, for 10278 observed reflections. The complexity of the crystal structure is based on different points, as the existence of: both "gauche" and "trans" conformations of the organic ligand, the $[V_{12}O_{36}]^{-12}$ cycles, formed by 12 corner-sharing VO_4 tetrahedra, and, finally, the combination of both three-dimensional metal−organic and inorganic substructures, giving rise to a self-catenated highly connected net. The crystallization water molecules are semi-encapsulated in the channels along the [100] direction, and their loss gives rise to a dynamical and reversible structural contraction. Moreover, after the removal of the crystallization water molecules, the compound exhibits a negative thermal behavior in the 85−155 °C temperature range, and irreversible structural transformation due to the loss of coordinated water molecules up to 200 °C. The IR and UV−vis spectra were determined for the as-synthesized sample, after the removal of crystallization water molecules and after the irreversible transformation due to the loss of coordinated water molecules. The thermal evolution of χ_m was adjusted to a magnetic model considering an isotropic dimer plus two Ni(II) d^8 isolated octahedra.

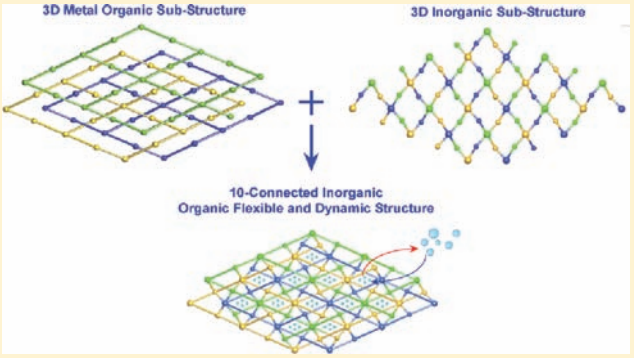

INTRODUCTION

In recent years, the analysis of topological networks and entanglements has been a interesting point of research in crystal engineering.[1] The interest in entangled systems, and concretely in self-catenated ones, is also rapidly increasing, not only for their potential applications as functional materials but also for their intriguing architectures and topologies. An entangled system is defined as an extended array more complex than its constituents, which is composed of individual motifs forming, via interlocking or interweaving, a periodic architecture infinite in at least one dimension. The different kind of entanglements (interpenetration, catenation, self-catenation) are systematically defined and described in the Carlucci et al. work.[2] Another interesting strategy to obtain porous materials in the construction of highly connected frameworks (namely, connectivities higher than six).[3] In that respect, these metal−organic frameworks are constructed from lanthanide metals or polynuclear mono or heterometallic clusters as building blocks.[4,5]

The combination of metal organic nets based on nitrogen donor dipodal ligands and vanadium oxide subunits has become a great strategy to obtain self-catenated and/or highly connected nets[6] and because of their potential application in catalysis,[7] hydrogen storage,[8,9] molecular adsorption,[10] electromagnetism,[11] and photochemistry,[12] among others. In the specific case of the vanadium oxides, recent interest has been focused on their potential use as secondary cathode materials for advanced lithium batteries[13] and their importance in the industrial oxidative catalysis and photocatalytic properties.[14]

Despite the difficulties to control the hydrothermal synthesis toward predictable crystal architectures, the analysis of the synergetic interaction between the inorganic and organic components, allows a partial degree of "crystal engineering", toward more open or condensed structural archetypes, and to more rigid or flexible response of the crystal structure to the loss or uptake of solvent.[15] The choice of bidentate ligands allows extended metal−organic subnets and high dimensionality open crystal structures to be obtained. To obtain extended hybrid frameworks, we have chosen Ni^{2+} because of the octahedral coordination preferences of this metal and bidentate ligands

Received: September 6, 2011
Published: February 3, 2012

   dx.doi.org/10.1021/ic201951e | *Inorg. Chem.* 2012, 51, 2130−2139

such as pyrazine (Pz), 4,4́-bipyridine (Bpy), 1,2-di(4-pyridyl)-ethene (Bpe), or 1,2-di(4-pyridyl)ethane (Bpa).[16,17] On the other hand, the modification of the hydrothermal synthesis conditions, such as time, temperature, stoichiometry, pH, concentration, and filling factor, allows a partial control of the oxoanion polymerization degree, giving rise to different stable $\{V_xO_y\}$ species stable in solution.[18] Examples of those are the $\{V_2O_7\}$ dimers, $\{V_4O_{12}\}$ cyclic tetramers, or $\{VO_3\}$ metavanadate chains.[19] In that respect, we have recently reported the effect of the initial concentration and pH value on the hydrothermal synthesis of the Ni/Bpy/V_xO_y and Ni/Bpe/V_xO_y systems.[20]

The thermal behavior of hybrid materials is closely related to the inherent flexibility of the crystal framework. This way, the dynamic and reversible response to the removal or uptake of solvent molecules reported for different MOFs is related to the existence of weak points within the different linkages of the structural subunits. In a parallel way, the NTE (Negative Thermal Expansion) behavior reported for the cyanide bridged compounds,[21] or more recently for several MOFs[22] arises principally in the thermal population of low-energy vibrational modes of the bridging ligands, and hence in the possibility of a flexible thermal response of the structural subunits. However, the studies of the thermal behavior of hybrid vanadates are still rare, despite that it is known that some of them exhibit a dynamical and reversible response of the crystal structure,[23] NTE,[24] near zero thermal expansion,[25] or structural irreversible transformations due to the loss of coordinated water molecules.

Here we report on the preparation and structural description of $[\{Ni_3(H_2O)_3(Bpa)_4\}(V_6O_{18})]\cdot 8H_2O$ 6,10-c self-catenated highly connected net, that combines both three-dimensional inorganic and metal−organic scaffolds. A dynamic and reversible response of the crystal structure to the loss of crystallization water molecules, negative thermal expansion up to 85 °C, together with an irreversible structural transformation due to the loss of lattice water molecules are described.

EXPERIMENTAL SECTION

Materials and Methods. The following chemicals were used as received with no further purification: 1,2-di(4-pyridyl)ethane (Bpa), $Ni(NO_3)_2\cdot 6H_2O$, $NaVO_3$ from Sigma-Aldrich, and 1 M HCl solution was prepared from a HCl solution 35% of Panreac. All synthetic reactions were carried out in 50 mL Parr Teflon-lined acid digestions bombs. A mixture consisting of $NaVO_3$ (0.0308 mmol), 1,2-di(4-pyridyl)ethane (0.0478 mmol), $Ni(NO_3)_2\cdot 6H_2O$ (0.0750 mmol), and H_2O (30 mL) in the molar ratio 1:1:1 was placed in a 50-mL Parr Teflon-lined autoclave. The initial pH value was adjusted to 6.5 with a 1 M HNO_3 solution under a vigorous stirring. The autoclave was sealed and heated for 3 days at 120 °C. After the reaction, a mixture of green single crystals of the title compound with yellow strongly twinned crystals and a pale green powder were obtained. The studied material was separated manually from the mixture, under a polarizing light microscope. The sample was washed and dried with acetone.

A great number of hydrothermal syntheses were carried out to obtain the title compound as a single phase. Modifications of the initial pH, stoichiometry, reaction time, filling factor, reaction temperature, and concentrations allowed us to crystallize four different nickel hybrid vanadates in this system. In all the studied conditions, the title compound cocrystallizes with other hybrid vanadates. Several factors could affect the outcome of the reaction; however, one of the most critical factors in this system is the initial $NaVO_3$/Bpa stoichiometry of the started reagents. The crystallization of one compound could modify the $NaVO_3$/Bpa ratio in solution, favoring the crystallization of a second phase during the hydrothermal treatment. This is a qualitative explanation of the studied hydrothermal reactions; however, a combination of several factors could be responsible of the outcome of the reaction.

The density was measured by flotation method in a mixture of bromoform/chloroform, being 1.66(1) gr cm^{-3}. Chemical analysis: Calcd. for $[\{Ni_3(H_2O)_3(Bpa)_4\}(V_6O_{18})]\cdot 8H_2O$: H 4.14, C 33.82, N 6.57, V 17.93, Ni 10.33%. Found: H 4.41, C 33.62, N 6.64, V 17.98, Ni 10.45%.

The samples were characterized by powder X-ray diffraction. The patterns were recorded on a Bruker ADVANCE Vårio diffractometer (CuKα1 radiation) (2θ range = 5−70°, step size = 0.015°, time exposure = 10 s per step). The Rietveld refinement with a fixed structural model, confirms the inexistence of impurities, despite of the problems in the fit of some reflections intensity because of the preferred orientation of the samples (Supporting Information, Figure S1). The final fit corroborates the purity of the sample that was used to measure the chemical and physical properties of the material (χ^2 = 2.02, R_f = 9.90, R_{Bragg} = 16.7).

Crystal Structure Analyses. Plate like single crystals of title compound were selected under a polarizing microscope and mounted on a glass fiber. Crystal data were collected at 293 K on a Xcalibur Nova diffractometer equipped with a Onyx detector and graphite-monocromated CuKα radiation. The Lorentz-polarization and absorption correction were made with the diffractometer software,[26] taking into account both the shape and crystal size.

The structure was solved in the monoclinic $P2_1/c$ space group by direct methods (SIR-92).[27] The refinements were performed by full-matrix least-squares based on F^2, using the SHELX97 program.[28] Anisotropic thermal parameters were used for all atoms except for the oxygen atoms of the crystallization water molecules and the hydrogen atoms belonging to the organic ligand, which were fixed geometrically and allowed to ride on their parent carbon atoms (C−H 0.93 Å (**1**) $U_{iso}(H) = 1.2U_{eq}(C)$ Å^2). The disorder of one ring of the Bpa molecules was solved making equal the chemical equivalent bond lengths and angles, but not torsion angles, of the two disordered rings. For this purpose the PART, SAME, SIMU, and SADI commands available in SHELXL97 were used. Equal anisotropic thermal displacements were used for the carbon and nitrogen atoms belonging to the disordered Bpa molecules to avoid unusual thermal ellipsoids. In the final steps of the refinement, an important residual density was located near the V(1) atom. The bond distances between the residual peak and the oxygen atoms belonging to the $V(1)O_4$ tetrahedra are in good agreement with the V−O bond distances for a four coordinated vanadium. A disorder of the $V(1)O_4$ polyhedra was modeled. V(1B) and O(14B) atoms were refined with isotropic thermal displacements, because of their low occupation factor 0.102(3). The hydrogen atoms belonging to the coordinated water molecules were located in the difference density map. The O−H and H−H distances were restrained to 0.92(1) and 1.35(2) Å values, respectively. Isotropic thermal parameters were used for the hydrogen atoms belonging to the coordinated water molecules. In the final steps of the refinement, eight disordered crystallization water molecules were located in the channels of the crystal structure. The hydrogen atoms belonging to the crystallization water molecules were not located. Details of crystal data, data collection and reduction, structure solution, and refinement are reported in Table 1. Further details of the crystal structure may be obtained from the CCDC by quoting the depository number 780947.

Physical Measurements. The infrared spectra were recorded on a Jasco FT/IR-6100 spectrometer with pressed KBr pellets in the range 4000−400 cm^{-1}. IR (KBr, ν/cm^{-1}): 3394(s), 3215(s), 3074(w), 2930(w), 1617(s), 1560(m), 1502(m), 1444(w), 1424(s), 1225(m), 1216(m), 1066(m), 1023(m), 936(f), 920(f), 821(f), 798(f), 698(f), 680(f), 664(f), 552(m), 530(w), 497(w). IR spectra of the pristine sample and after heating this one up to 25, 50, 100, 150, 200, 250 °C were also registered. In a parallel way, diffuse reflectance spectra were recorded on a Varian Cary 50000 spectrophotometer in the 50000−4000 cm^{-1} range. UV−vis spectra were registered for the as-synthesized sample, and after heating this one at 100 and 160 °C during one day.

Thermogravimetric analysis was performed in air atmosphere, up to 500 °C, with a heating rate of 5 °Cmin^{-1} on a DSC 2960 Simultaneous DSC-TGA TA Instrument. The temperature-dependent PXRD in air atmosphere was performed on a PHILIPS XPERT PRO diffractometer (CuKα radiation), equipped with a variable-temperature stage (Anton Paar Physica TCU2000) with a Pt sample holder. Patterns were

dx.doi.org/10.1021/ic201951e | Inorg. Chem. 2012, 51, 2130−2139

Table 1. Crystal Data and Structure Refinement

	$\{Ni_3(H_2O)_3(Bpa)_4\}(V_6O_{18})]\cdot 8H_2O$
formula	$C_{48}\ H_{54}\ N_8\ Ni_3\ O_{29}\ V_6$
Fw (g/mol)	1688.76
crystal system, space group	monoclinic, $P2_1/c$
a (Å)	13.5536(2)
b (Å),	19.0463(2)
c (Å)	27.7435(3)
β (deg)	112.3880(10)
Z, $F(000)$, temperature (K)	4, 3408, 293
μ (mm^{-1})	8.446
ρ_{calc}, $\rho_{obs.}$ (gr/cm^3)	1.694, 1.67(1)
crystal size (mm), crystal color	0.12 × 0.05 × 0.03, green
radiation (λ(Å))	1.5418
nos. of reflns., indep. reflns.	50933, 13347
h, k, l inter	$-16 \geq h \geq 16$, $-16 \geq k \geq 23$, $-34 \geq l \geq 34$
R(int), $R(\sigma)$	0.0613, 0.0535
R1, wR2(obs) ($I > 2\sigma(I)$)	0.0558, 0.1359
R1, wR2(all)	0.0731, 0.1446
GooF S	0.995
no. of parameters/restraints	862, 29
l. diff. peak (e $Å^{-3}$), l. diff. hole (e $Å^{-3}$)	1.176, −1.09

recorded each 10 °C from 25 to 505 °C (2θ step = 0.0263°, 2θ range = 5−17°, exposure time = 1 s per step). To corroborate the reversibility of the heating response of the crystal structure, patterns were recorded at 100, 150, 200, 250 °C and after lowering the temperature to 30 °C and adding distilled water to the preheated samples. In a second attempt, and to corroborate the NTE behavior of the dehydrated compound, the pristine sample was heated at 130 °C during 30 min under vacuum, and then a thermodiffractometric experiment of the dehydrated compound under vacuum was carried out. The patterns were recorded each 25 °C from 30 to 255 °C (2θ step = 0.0333°, 2θ range = 5−8°, time exposure = 5 min per pattern).

Magnetic measurements on powdered samples were performed in the temperature range 2−300K, using a Quantum Design MPMS-7 SQUID magnetometer. The magnetic field was 0.1T, a value in the range of linear dependence of magnetization vs field, even at 2 K.

RESULTS AND DISCUSSION

Crystal Structure. The crystal structure of the compound exhibits a three-dimensional (3D) framework constructed from 3D metal−organic and inorganic substructures, whose combination gives rise to an unprecedented 6,10-c self-catenated net. The connectivity between the Ni(II) ions and the Bpa ligands generates a $\{Ni_3(H_2O)_3(Bpa)_4\}^{6+}$ metal−organic subnet constructed from three interpenetrating 3D nets, Class Ia, FIV [0,1,0], shown in Figure 1 d. Each metal organic net is generated from the connectivity between the tetrameric units and $Ni(2)N_4O_2$ through "trans" conformation Bpa ligands (Supporting Information, Figure S2). The tetrameric unit consists of two edge sharing octahedra forming $Ni(1)_2N_4O_4(H_2O)_2$ dimers linked to two $Ni(3)N_2O_2(H_2O)_2$ octahedra through Bpa ligands in "gauche" conformation (Figure 1 b). Each tetrameric unit is linked to four $Ni(2)N_4O_2$ octahedra via trans-Bpa ligands. The $Ni(2)N_4O_2$ octahedra are four connected, and link two tetrameric units and two $Ni(2)N_4O_2$ via the "trans" organic ligand. (Figure 1 a). The connectivity between the tetrameric units and the $Ni(2)N_4O_2$ octahedra through the Bpa ligand generates a "mot" like metal organic net (Figure 1 c). The simplified metal organic net can be described as a 3D+3D+3D interpenetration of two nodal $(4\text{-c})_2(4\text{-c})$ nets with "mot" like topology and $\{6^4.8^2\}_2\{6^2\}$ point symbol (Figure 1 d). Scheme 1 shows the two possible conformations for the Bpa organic ligand.

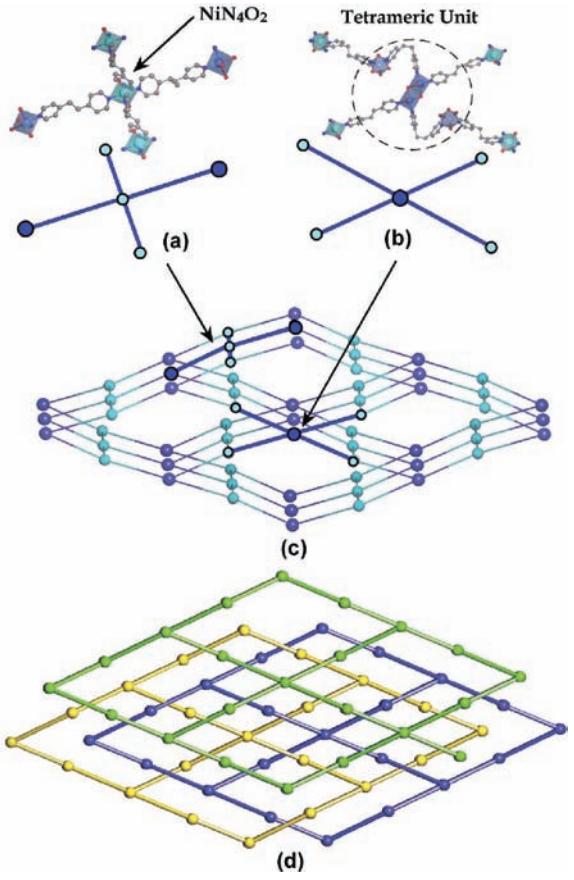

Figure 1. (a) $Ni(2)N_4O_2$ octahedra linked to other two $Ni(2)N_4O_2$ octahedra and two tetrameric units. The simplification is a four connected node. (b) The tetrameric unit formed by the $Ni(1)_2N_4O_4(H_2O)_2$ dimers and two $Ni(1)_2N_4O_4(H_2O)_2$ octahedra linked by the Bpa ligands in "gauche" conformation. (c) The "mot" like 3D metal organic network generated by the joint of tetrameric units and $Ni(2)N_4O_2$ octahedra through tetrameric units. (d) Interpenetration of the three "mot" like metal organic frameworks. The colors of the nodes are related to the different metal organic frameworks and are maintained in Figures 3 and 4.

Scheme 1. "Trans" and "Gauche" Conformations for the 1,2-Di(4-pyridyl)ethane Organic Molecule

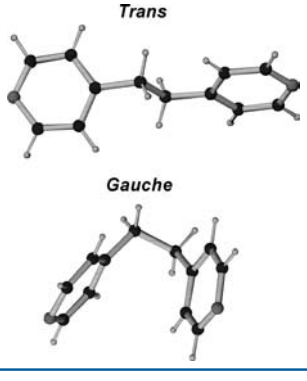

The anionic $[V_{12}O_{36}]^{-12}$ metallocycle is constructed from 12 corner sharing $\{VO_4\}$ tetrahedral units (Figure 2). The $Ni(1)_2N_4O_4(H_2O)_2$ dimers, belonging to the tetrameric units,

dx.doi.org/10.1021/ic201951e | Inorg. Chem. 2012, 51, 2130−2139

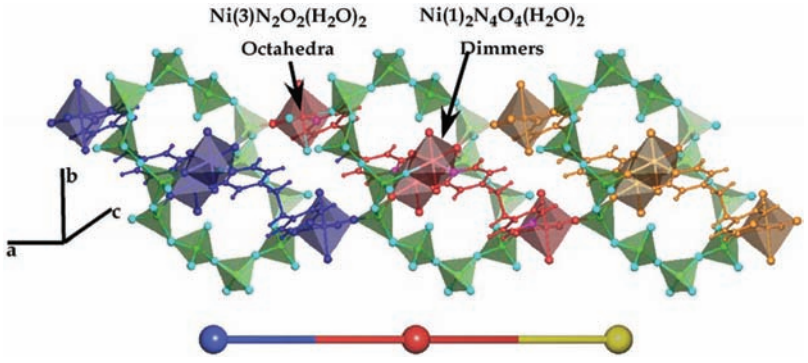

Figure 2. Inorganic–organic chains generated from the combination of the tetrameric units and the $V_{12}O_{36}$ cycles (green polyhedra).

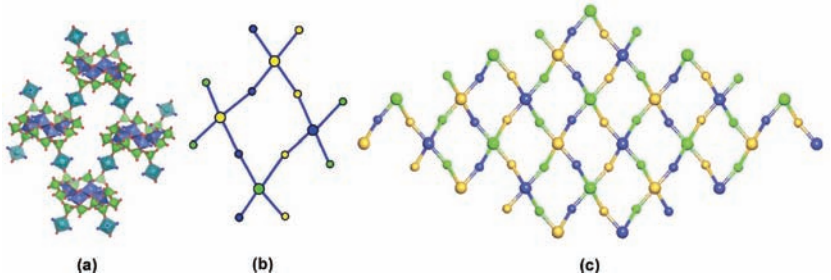

Figure 3. (a) Inorganic chains linked through $Ni(2)N_4O_2$. (b, c) Simplification of the inorganic substructure. The large circles represent the inorganic chains and the small ones the $Ni(2)N_4O_2$ octahedra. The colors of the nodes are the same that those in Figure 1d, and are common for the nodes belonging to the same metal–organic net.

lie inside the $[V_{12}O_{36}]$ cycles, linked via corners to two VO_4 tetrahedra, and generating $\{Ni(1)_2N_4O_4(H_2O)_2[V_{12}O_{36}]\}$ clusters (Figure 2). Those clusters are linked by the $Ni(3)N_2O_2(H_2O)_2$ octahedra, which are also shared with the dimeric units through "gauche" conformation Bpa ligands. Hence, each $[V_{12}O_{36}]^{-12}$ metallocycle contains one tetrameric unit that acts as a linker between adjacent metallocycles (Supporting Information, Figure S3).

The simplified chain is constructed from the connection by corners of unprecedented inorganic–organic heterometallic $[\{Ni_4O_8(H_2O)_4(Bpa)_2\}(V_{12}O_{36})]$ nodes, involving one tretrameric unit and one $[V_{12}O_{36}]^{-12}$ metallocycle (Figure 2). Curiously, the simplified inorganic chains has the same topology as the inorganic–organic ones; however, the nodes consist of heterometallic $[\{Ni_4N_8O_8(H_2O)_4\}(V_{12}O_{36})]$ clusters (Figure 2). The $[\{Ni_4N_8O_8(H_2O)_4\}(V_{12}O_{36})]$ units are six connected inorganic clusters. Those are connected to four $Ni(2)N_4O_2$ (Figure 3a) and to other two inorganic clusters belonging to the inorganic chains. Figure 3b shows the simplification of the inorganic substructure shown in Figure 3 a). The $Ni(2)N_4O_2$ octahedron links two inorganic chains. The connectivity between the inorganic subunits generates a 3D inorganic substructure with an unprecedented two nodal $(2\text{-c})_2(6\text{-c})$ $\{6^8.8^5.10^2\}\{6\}_2$ topology.

The combination of the "mot" like metal–organic net and the $(2\text{-c})_2(6\text{-c})$ inorganic framework, generates an unprecedented $(4\text{-c})_2(4\text{-c})+(2\text{-c})_2(6\text{-c})\rightarrow(6\text{-c})_2(10\text{-c})$ connected net, with $\{4^{12}.5.6^2\}_2\{4^{24}.5^{10}.6^{11}\}$ point symbol (Figure 4 and Supporting Information, Figure S4). The inorganic–organic clusters are a new example of 10-c connected nodes, which are linked to four $Ni(2)N_4O_2$ octahedra of the same metal–organic framework through the Bpa ligand, to two other clusters belonging to the inorganic chains, and to four $Ni(2)N_4O_2$ octahedra, which belong at the same time to the other two metal

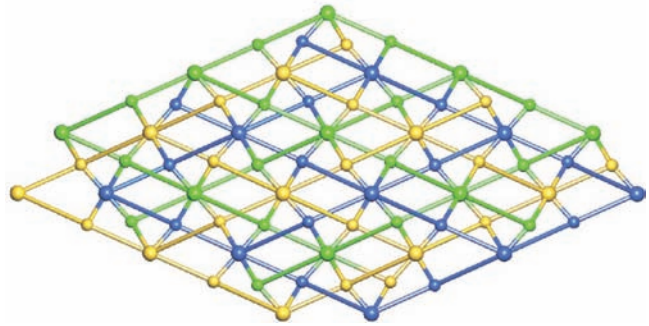

Figure 4. Simplification of the crystal structure considering both the metal–organic and the inorganic substructures. The colors of the nodes are the same that those in Figure 1d, and are common for the nodes belonging to the same metal–organic net.

organic frameworks through the $V_{12}O_{36}$ metallocycle (Supporting Information, Figure S3b,c).

Table 2 depicts the bond distances related to the inorganic scaffold of the crystal structure. The coordination spheres of the Ni(II) and V(V) cations are near the ideal geometries for the octahedron and tetrahedron, respectively. The Ni–O bond lengths range from 2.180(3) Å for Ni(2)–O(3W)^{vi} to 2.002(3) Å for Ni(2)–O(10) (vi = $-x+1, -y+1, -z$); while the Ni–N bond distances range from 2.136(3) Å for Ni(3)–N(8)^{x} ($x = -y+1/2, z-1/2$) to 2.063(11) Å for Ni(1)–N(1)B. The bond distances related to the coordinated water molecules are slightly longer than those for the nitrogen and oxygen atoms. The V–O bond lengths are strongly dependent on the oxygen atom connectivity. From this point of view, the shorter V–O bonds are related to the terminal oxygen atoms which are corner-linked to the nickel(II) cation. The V–O bonds with the oxygen atom shared by VO_4 tetrahedra possess slightly longer distances (see Table 2). The

dx.doi.org/10.1021/ic201951e | Inorg. Chem. 2012, 51, 2130–2139

Table 2. Selected Bond Distances (Å)[a]

Nickel Octahedra			
Ni1—N1A	2.080(9)	V1B—O16	2.003(7)
Ni1—N1B	2.063(11)	V1B—O13	1.590(7)
Ni1^{iii}—O13	2.037(3)	V1B—O14B	1.56(3)
Ni1—O1W	2.100(3)	V1B—O15	1.804(7)
Ni1—O2W	2.113(3)		
Ni1—O13^{iii}	2.037(3)	V2—O2	1.648(2)
Ni1—N5^{iii}	2.108(4)	V2—O16	1.791(3)
		V2—O5	1.634(3)
Ni2—O9	2.003(3)	V2—O6	1.799(3)
Ni2— O10	2.002(3)		
Ni2—N6	2.071(3)	V3—O6	1.819(3)
Ni2—N7	2.072(3)	V3—O10^{vi}	1.652(3)
Ni2—O3W	2.153(3)	V3—O7	1.615(3)
Ni2—O3W^{vi}	2.180(3)	V3—O8	1.813(3)
		V4—O12	1.643(3)
Ni3—N8^{x}	2.136(3)	V4—O8	1.778(3)
Ni3—O1^{vii}	2.054(2)	V4—O9	1.646(3)
Ni3—O2	2.059(3)	V4—O11	1.785(3)
Ni3—N2^{viii}	2.090(3)		
N3—Ni3	2.106(3)	V5—O3	1.633(3)
Ni3—N4^{ix}	2.110(3)	V5—O4	1.773(3)
		V5—O11	1.811(3)
Vanadium Tetrahedra		V5—O1	1.653(2)
V1A—O14A	1.620(4)	V6—O17	1.620 (4)
V1A—O13	1.670(3)	V6—O18	1.640(4)
V1A—O15	1.742(4)	V6—O4	1.793(3)
V1A—O16	1.805(3)	V6—O15^{vi}	1.799(4)

[a]Symmetry codes: (i) $x, y-1, z$; (ii) $x-1, y, z$; (iii) $-x+2, -y+1, -z$; (iv) $x, -y+1/2, z+1/2$; (v) $-x+1, y-1/2, -z-1/2$; (vi) $-x+1, -y+1, -z$; (vii) $-x+1, y+1/2, -z-1/2$; (viii) $x, y+1, z$; (ix) $x+1, y, z$; (x) $x, -y+1/2, z-1/2$.

bond valence calculations assuming V(V)—O, Ni(II)—O and Ni(II)—N bonds are depicted in Table 3, and give values near the expected 5+ and 2+ oxidation states for the vanadium and nickel atoms, respectively.

Table 3. Bond Valence Sum Parameter for Nickel, Vanadium, Oxygen, and Nitrogen Atoms

atom	charge	atom	charge	atom	charge
Ni(1)	2.001	O(5)	2.136	O(18)	1.571
Ni(2)	2.017	O(6)	1.969	Ow(1)	1.674
Ni(3)	2.000	O(7)	1.802	Ow(2)	1.665
V(1A)	5.247	O(8)	2.168	Ow(3)	1.864
V(2)	5.149	O(9)	2.048	N(1A)	3.050
V(3)	5.086	O(10)	2.019	N(1B)	3.056
V(4)	5.170	O(11)	2.025	N(2)	3.114
V(5)	5.131	O(12)	2.030	N(3)	3.153
V(6)	5.257	O(13)	2.052	N(4)	3.116
O(1)	2.093	O(14)	1.640	N(5)	3.084
O(2)	2.262	O(15)	2.191	N(6)	3.132
O(3)	1.849	O(16)	2.161	N(7)	3.141
O(4)	2.112	O(17)	1.777	N(8)	3.087

The complexity of the crystal framework is based on the highly ten connected nodes. This fact is promoted by several aspects such as, the presence of "gauche" and "trans" conformation Bpa molecules in the same crystal structure, the existence of unprecedented $[V_{12}O_{36}]^{-12}$ metallocycles and metal—organic tetrameric units, and finally the combination of both the inorganic and organic scaffolds. As far as we are aware, this is the second example of hybrid vanadate combining both 3D inorganic and organic frameworks.[29]

The crystal structure possesses channels along the [100] direction, in which the disordered crystallization water molecules are located. The construction of the VDP (Voronoi—Diritchlet polyhedra)[30] for the crystallization water molecules reveals that these ones are partially confined between the organic molecules and the inorganic framework. These crystallization water molecules are semi-encapsulated into two points with volumes of 43.1 and 348.2 Å^3 (Supporting Information, Figure S5), and a total volume per formula unit of 434.4 Å^3. The channel's closest section is of 4.8 × 5.0 Å.

Thermal, Spectroscopic, and Magnetic Properties. The thermal stability of $[\{Ni_3(H_2O)_3(Bpa)_4\}(V_6O_{18})]\cdot 8H_2O$ was studied by thermogravimetric and thermodiffractometric measurements. The TGA and DSC curves (Supporting Information, Figure S6) exhibit three weight loss processes. Between 25 and 120 °C the loss of the crystallization water molecules takes place. The observed weight loss (Obs. 12.4%) is higher than that of the calculated from the removal of crystallization water molecules (Calc. 8.45%), indicating that the process is overlapped with the loss of adsorbed water. The thermal decomposition is initiated by the loss of coordinated water molecules (Obs. 4.1%, Calc. 3.17%). The observed weight loss in the 225—310 °C temperature range corresponds to three water molecules per formula unit. Finally, the weight loss (42.1%) occurring at 350—490 °C is related to the calcination of four Bpa organic molecules per formula unit (Calc. 43.2%).

The thermal stability was also studied by time-resolved X-ray thermodiffractometry in air atmosphere (Supporting Information, Figure S7). The thermodiffractometric measurement shows important displacements of the diffraction maxima position during the heating process (Supporting Information, Figure S7). The peak fit of the (110), (002), and (100) maxima allow us to determine the thermal variation of intensity and 2θ (deg) position for these reflections (Figure 5). In a parallel way, and to determine the thermal evolution of the cell parameters, the pattern matching analyses of the different patterns were carried out; however, the changes observed in the crystal structure are high enough to give rise to a poor fit up to 160 °C.

Both the shift of the (110) maximum and the cell parameters evolution suggest three different tendencies during the heating process, in good agreement with the TG/ATD measurement.

The first process occurs between room temperature and 85 °C, and gives rise to an important increase of the (110) reflection intensity and important shift of the (002) maximum from 6.70 → 6.88° in 2θ. The temperature range is related to the loss of crystallization water molecules. This process generates the reduction of the "c" parameter, as judged by the (002) maximum displacement, which indicates a contraction of the [100] channels in which the crystallization water molecules were located. The intensity increase of the (110) reflection also suggests important structural changes of the host during the release of crystallization water molecules.

From 85 to 155 °C, the (110), (002), and (100) reflections shift their positions from 5.55° → 5.75°, 6.80° → 6.95°, and 6.90 → 7.40° in 2θ, respectively. The (002) maximum also lost intensity progressively. As judged by the thermal displacements of the three strongest reflections, the crystal structure continues its contraction after the removal of the crystallization water molecules. This fact suggests that the dehydrated compound exhibits a negative thermal expansion (NTE) behavior.

dx.doi.org/10.1021/ic201951e | Inorg. Chem. 2012, 51, 2130—2139

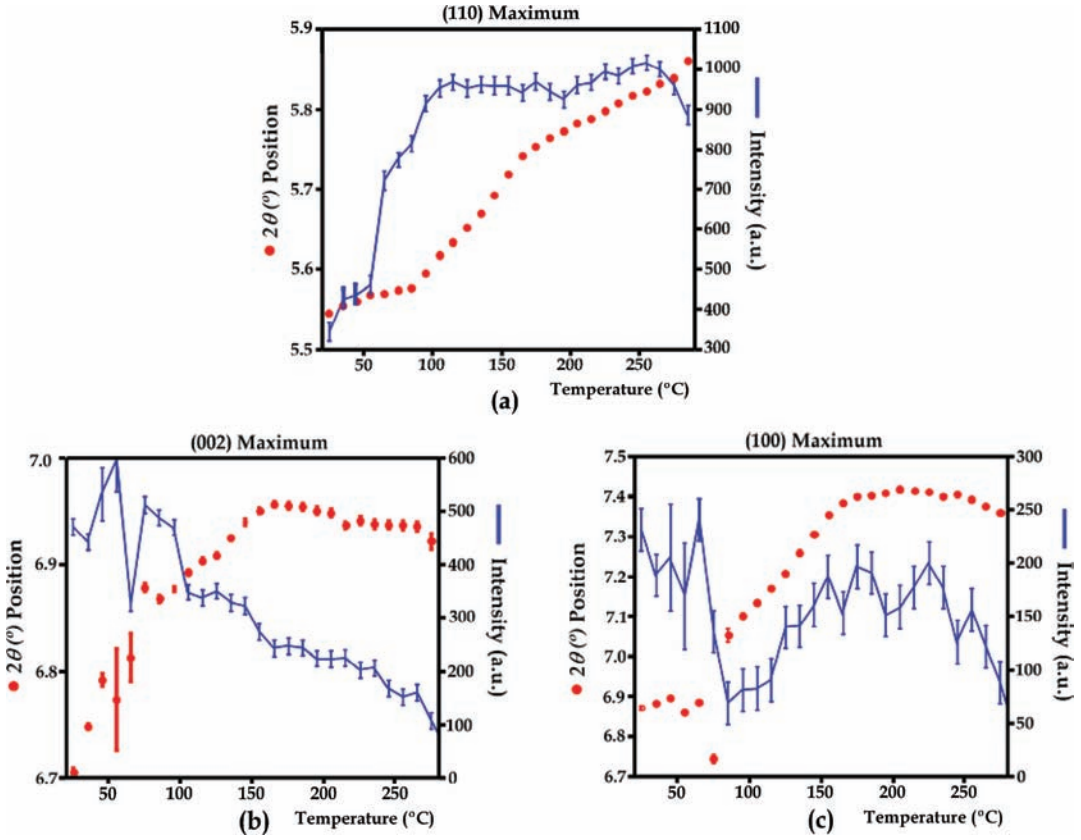

Figure 5. Intensity and 2θ (deg) position determined from Peak fit of (110), (002), and (100) maxima.

In the 200−275 °C temperature range the diffraction patterns show a continuous loss of crystallinity of the maxima located at 2θ (deg) values higher than 6°. The loss of coordinated water molecules during this temperature range generates an irreversible and strong structural transformation. This fact probably implies a strong structural reorganization, promoting a reduction of the crystal domains diminishing the crystallinity of the patterns. Finally, upon 275 °C the structural collapse because of the calcination of the organic ligand takes place.

To corroborate the reversibility of the heating response of the crystal structure, patterns were recorded at 100, 150, 200, 250 °C and after lowering the temperature to 30 °C and adding distilled water to the preheated samples. The results are summarized in Supporting Information, Figure S8. The patterns are completely reversible in the sample heated up to 150 °C, indicating that both the loss of crystallization water molecules and the negative thermal expansion between 85 and 155 °C are completely reversible. The samples heated at 200 °C recover partially the position of the diffraction maxima. However, the pattern of the sample heated at 250 °C is equal to the same one recorded after cooling it to 30 °C, revealing the existence of an irreversible process during the loss of coordinated water molecules.

One of the most interesting features of the title compound is the negative thermal expansion in the 85−155 °C temperature range. The TG and ATD curves present a minor weight loss in this temperature range, while the crystal structure experiments a 6.24% of the volume cell reduction. The thermal evolution of the (011) reflection for the dehydrated compound corroborates the NTE behavior after removing the crystallization water molecules (Supporting Information, Figure S9). Up to 180 °C, the removal of crystallization water molecules generates a second maxima near the (001) one, that increases progressively its intensity.

The IR spectrum of the title compound presents the characteristic absorption bands corresponding to the vibration modes of the water molecules (Figure 6a), the Bpa organic ligand (Figure 6b) and $(VO_4)^{-3}$ vanadate anion, which appear in the 1600−1000 and 950−530 cm^{-1}, ranges, respectively (Figure 6 c,d).

The IR spectra collected after treating the sample at 200 and 250 °C show significant changes in the absorption bands related to the $V_{12}O_{36}$ cycles, suggesting an important structural reorganization after the loss of the coordinated water molecules. The absorption bands related to the crystallization and coordination water molecules lose intensity progressively with increasing temperature (Figure 6a). The loss of coordinated water molecules (up to 200 °C) gives rise to displacements and intensity reduction of the absorption bands related to the V=O terminal bonds (Figure 6 c). Minor changes in the width and intensity of the absorption bands related to the Bpa ligand are also observed (Figure 6 b). The intensity loss of the absorption maxima related to the V−O−V and V−O−Ni antisymmetric modes are probably related to the loss of crystallinity during the release of the coordinated water molecules (Figure 6d).

In the diffuse reflectance UV−vis spectrum (Figure 7), two strong absorption bands corresponding to the allowed transitions $^3A_{2\ g}(^3F) \rightarrow {}^3T_{2\ g}(^3F)$ and $^3A_{2\ g}(^3F) \rightarrow {}^3T_{1\ g}(^3F)$ at 9050 and 14975 cm^{-1}, and one shoulder due to the forbidden one $^3A_{2\ g}(^3F) \rightarrow {}^1E_{1\ g}(D)$ at 12930 cm^{-1} are observed. From these transitions corresponding to the d^8-high spin Ni(II) cation in octahedral geometry, the Dq and Racah *B* and *C* parameters have been calculated, by using the energy expressions given in

dx.doi.org/10.1021/ic201951e | *Inorg. Chem.* 2012, 51, 2130−2139

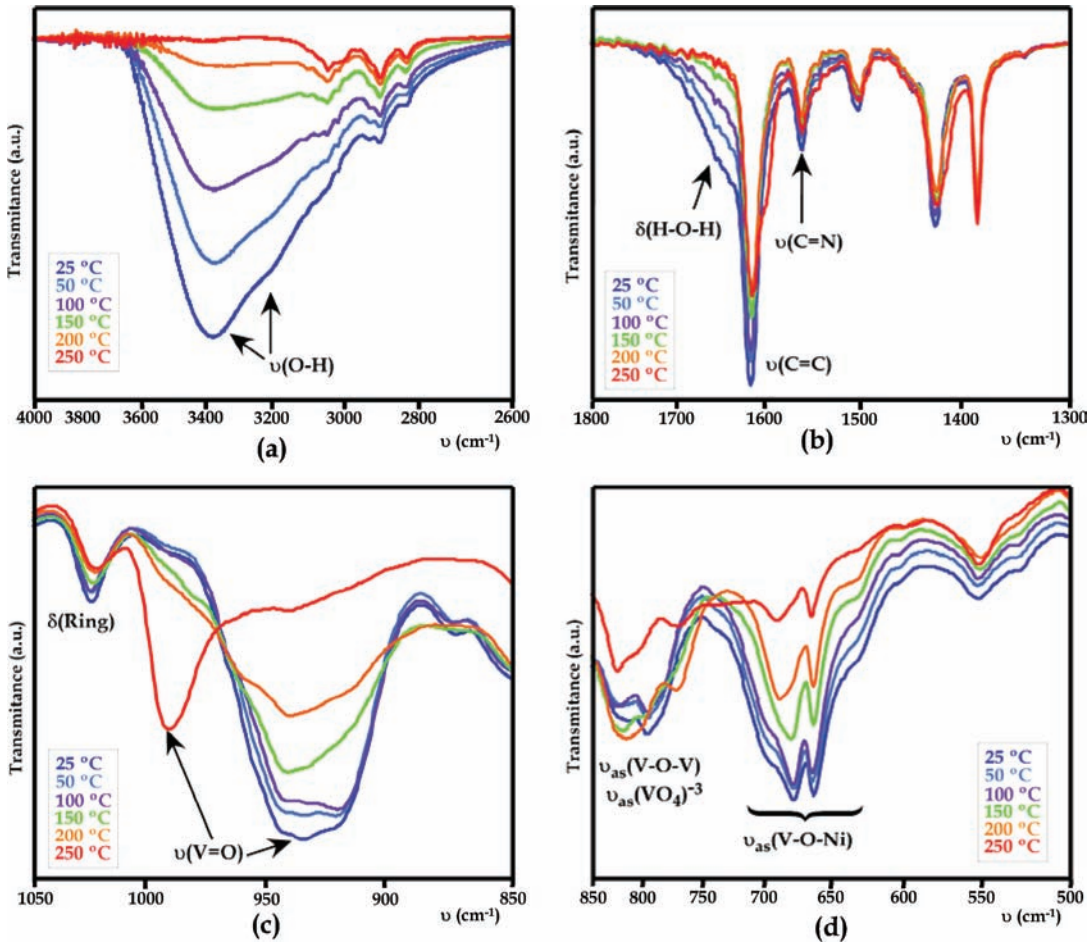

Figure 6. Infrared spectra for the pristine sample and heated at 25, 50, 100, 150, 200, 250 °C for 1 h.

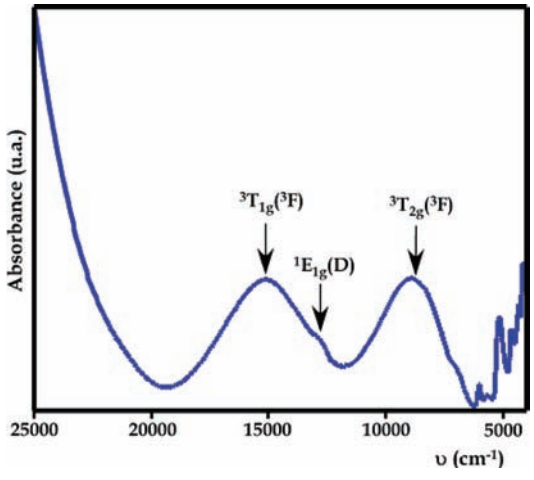

Figure 7. UV−vis spectra for the title compound.

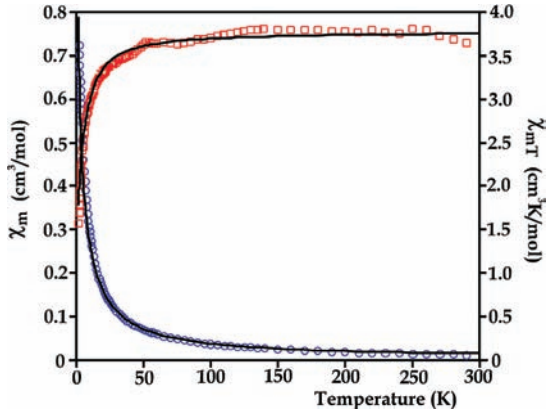

Figure 8. χ_m and χ_mT thermal evolution. The line is the best fit considering a magnetic model constructed from a half dimeric unit plus two isolated octahedra.

the Tanabe−Sugano diagrams.[31] The obtained values are Dq = 905, B = 940 cm^{-1}, and C = 3053 cm^{-1}. The value of the B-parameter is approximately 91% of the free Ni(II) cation (1030 cm^{-1}), which indicates an appreciable covalent character in the chemical bonds for the nickel octahedra.

Magnetic measurements for the title compound were performed on a powdered sample from room temperature to 2 K, at a magnetic field of 0.1 T. The thermal evolution of the molar magnetic susceptibility, χ_m, and χ_mT is shown in Figure 8. The χ_mT value at 300 K is 3.6 cm^3 K mol^{-1}, 1.2 cm^3 K mol^{-1} per nickel atom, near the expected (1.21 cm^3 K mol^{-1}) for non-interacting Ni(II) (S = 1, g = 2.2) ions. The χ_m curve shows a continuous increase of its value from 300 K (0.0119 cm^3 mol^{-1}) to 2 K (0.7234 cm^3 mol^{-1}).

Taking into account the disposition of the metal centers in the crystal structure, two different magnetic interactions are possible. The first one is the magnetic exchange between the nickel atoms of the $Ni(1)_2N_4O_4(H_2O)_2$ dimeric units (3.342 Å), and the second one is the magnetic exchange between the dimeric units and the nickel octahedra through

dx.doi.org/10.1021/ic201951e | Inorg. Chem. 2012, 51, 2130−2139

the organic ligand and vanadium oxide subunit. The distance between metal centers is higher than 6 Å, and the magnetic exchange pathway involves at least four atoms; so, significant exchange interactions are not expected.

Therefore, the thermal evolution of the magnetic susceptibility data can be attributed to the magnetic exchange interaction within the dimeric units plus the zero field splitting, typical for the axially distorted d^8 high spin isolated Ni(II) system (eq 1).

$$\chi_m = \frac{2N\beta^2 g^2}{kT}\frac{1 + 5\exp(4x)}{3 + 5\exp(4x) + \exp(-2x)} + 2\frac{2N\beta^2 g^2}{kT}\frac{(2/y) - ((2\exp(-y)/y) + \exp(-y)}{1 + 2\exp(-y)} \quad (1)$$

where $x = J/kT$, $y = D/kT$, N is Avogadro's number; β, Bohr magneton; g, gyromagnetic ratio; k, Bolzmann's constant, and T, absolute temperature. The best fitting parameters obtained are $g = 2.24$ $J/k = -4.7$ K and $D/k = -10.6$ K. The antiferromagnetic behavior of the title compound is similar to those observed in other octahedrally coordinated Ni (II) complexes with similar binuclear cores. Most of the magneto-structural correlations for binuclear Ni(II) complexes are based on the work of Nanda et al.[32] This work indicates a linear relationship between J and Ni−O−Ni bridging angle in Ni(II) dimers. A bridging angle of 97° is the crossover point between ferromagnetic and antiferromagnetic behavior coupling. From this point of view, the Ni(1)−O_w(3)−Ni(1) angle in the title compound with a 100.95° value favors the antiferromagnetic interaction between the metal centers, in good agreement with the obtained −4.7K exchange coupling. The D parameter value for the isolated Ni(II) centers is consistent with the observed distorted octahedral coordination environment, and fits well with the generally observed rather broad range from 22 to 12 cm^{-1}.

Final Remarks. The crystal structure complexity of the title compound is based on the combination of polymeric

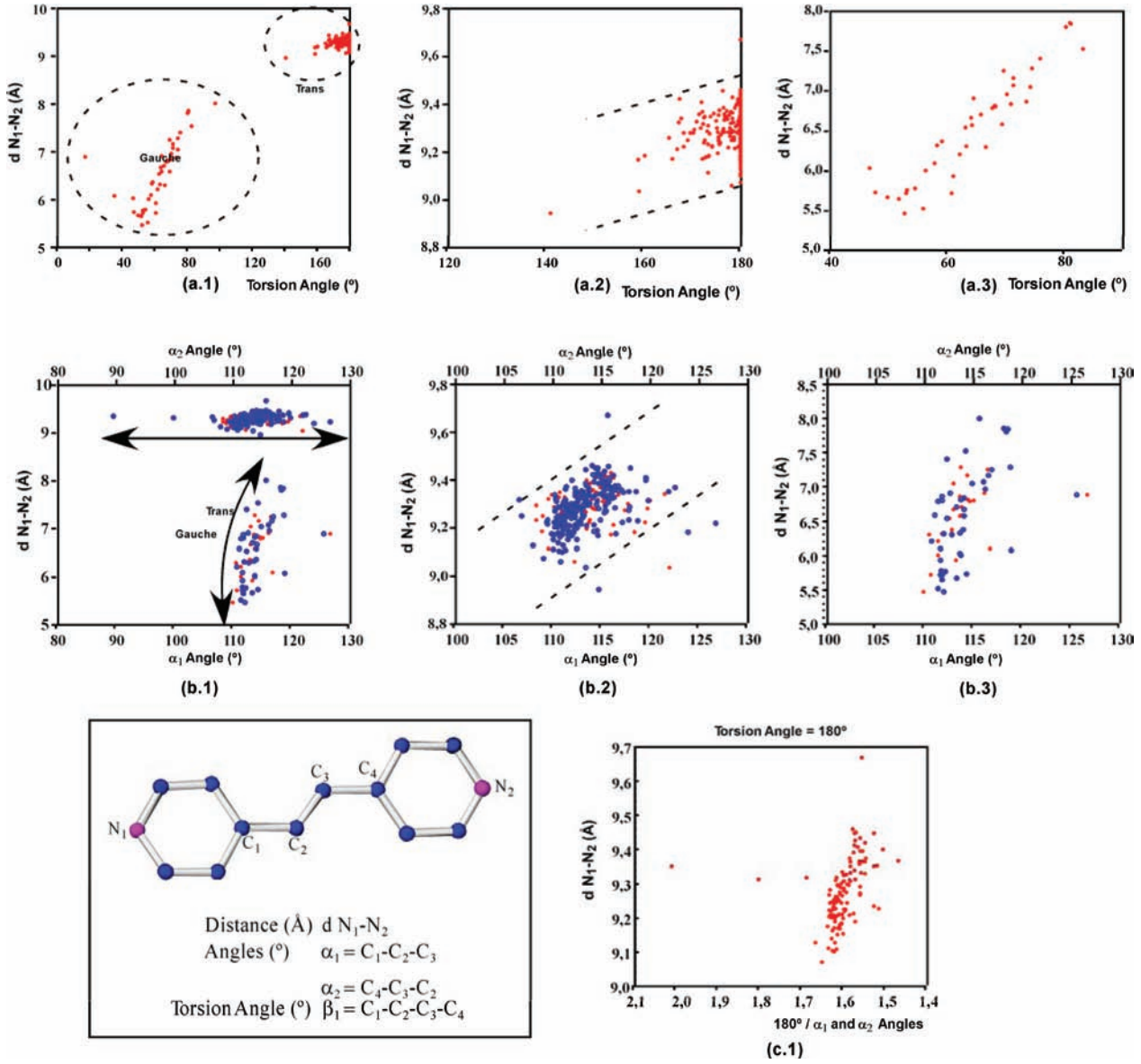

Figure 9. Crystal chemistry of the Bpa ligand. (a.1) Torsion angle vs d N1−N2 (a.2) for "trans" conformation and (a.3) "gauche" conformation. (b.1) $\alpha 1$ and $\alpha 2$ angles vs d N1−N2 (b.2) for "trans" conformation and (b.3) "gauche" conformation. (c.1) Effect of $\alpha 1$ and $\alpha 2$ angles in the d N1−N2 distance for the Bpa ligands with torsion angle equal to 180°.

dx.doi.org/10.1021/ic201951e | Inorg. Chem. 2012, 51, 2130−2139

metal−organic subnet with $V_{12}O_{36}$ vanadium oxide subunit. The synergetic interaction between them gives rise to the existence of both three-dimensional metal−organic and inorganic scaffolds in the same crystal architecture. Moreover, the title compound presents a dynamical and reversible response of the host to the removal of crystallization water molecules, and NTE behavior after releasing the solvent.

To determine the crystal structure mechanisms that generate this flexible response several single-X-ray diffraction experiments were carried out at high temperatures. However, the size of the single crystals, and the reduction of the intensity of the reflections after the loss of crystallization water molecules do not allow obtaining any data of enough quality to determine the crystal structure. Two important characteristics of the crystal framework that could allow the observed contraction during the loss of crystallization water molecules and the subsequent NTE behavior at higher temperatures can be considered: (i) the $[V_{12}O_{36}]^{-12}$ cycles are corner linked through nickel octahedra. In this way, the reorientation of the nickel octahedra during the loss of crystallization water molecules and the subsequent negative thermal expansion could explain the flexibility of the inorganic substructure. (ii) the Bpa organic ligand presents two different conformations in the crystal structure (see Scheme 1). To understand this behavior, a statistical analysis of the crystal structures containing the Bpa ligand from the CSD database was carried out.[33] The results of these analyses show that the variation of the torsion angles and C−C−C angles related to the ethane group could give rise to an important shortening of the N−N distance. The values of the torsion angle and the N−N distance depend on the ligand conformation; however, an important range of values is observed (Figure 9a.1). For the "trans" conformation the N−N distance varies from 9.5 to 8.9 Å, and slightly depends on the torsion angle value (Figure 9a.2). For the "gauche" conformation the N−N distance is strongly dependent on the torsion angle value. The N1−N2 distance takes values from 5.5 to 8.0 Å for torsion angles of 42 and 85°, respectively (Figure 9a.3). The C−C−C angles are also limited approximately between 105 and 125° (Figure 9b.1). For the "trans" conformation Bpa ligands a slight decrease of the N−N distance associated to the decrease of the C−C−C angles is observed (Figure 9b.2). In the case of the "gauche" conformation, the increase of the N−N distance in the Bpa ligands is principally related to the torsion angle; however, for larger N−N distances, a slight increase of the C−C−C angle is observed (Figure 9b.3). The C−C−C angles for the Bpa ligands with torsion angle equal to 180° clearly show that an increase of the angle value generates an increase of the N−N distance varying from 9.1 to 9.5 Å (Figure 9c.1). In conclusion, both the reorientation of the inorganic substructure and the organic ligand allow this flexible behavior of the crystal structure.

■ ASSOCIATED CONTENT

Ⓢ Supporting Information

(1) Rietveld refinement. (2) Interpenetration of three 3D "mot" like metal organic frameworks. (3) Ten connected clusters. (4) Crystal structure. (5) VDP polyhedra. (6) TG/DSC Curve. (7) Thermodiffractometry. (8) Reversibility. (9) Thermodiffractometry of the dehydrated compound. (10) Crystallographic information files (CIF). This material is available free of charge via the Internet at http://pubs.acs.org.

■ AUTHOR INFORMATION

Corresponding Author

*E-mail: maribel.arriortua@ehu.es-. Phone: 34-946012162. Fax: 34-946013500.

Notes

The authors declare no competing financial interest.

■ ACKNOWLEDGMENTS

This work has been financially supported by the "Ministerio de Educación y Ciencia" (MAT2010-15375) and the "Gobierno Vasco" (IT-177-07 and IT-312-07), which we gratefully acknowledge. The authors thank the technicians of SGIker (UPV/EHU), Drs. J. Sangüesa, I. Orue, P. Vitoria, and A. Larrañaga, financed by the National Program for the Promotion of Human Resources within the National Plan of Scientific Research, Development and Innovation, "Ministerio de Ciencia y Tecnología" and "Fondo Social Europeo" (FSE), for the X-ray diffraction and magnetic measurements, respectively. R.F.d.L. thanks the MEC (Madrid, Spain) (BES-2005-10322) and Universidad del País Vasco/EHU for funding.

■ REFERENCES

(1) (a) Blatov, V. A.; Carlucci, L.; Ciani, G.; Proserpio, D. M. *CrystEngComm* **2004**, *6*, 377−395. (b) Batten, S. R.; Robson, R. *Angew. Chem., Int. Ed.* **1998**, *37*, 1460−1494. (c) Blatov, V. A.; Carlucci, L.; Ciani, G.; Proseropio, D. M. *CrystEngComm* **2004**, *6*, 378−395. (d) Delgado-Friedrichs, O.; ÓKeeffe, M. *J. Solid State Chem.* **2005**, *178*, 2480−2485.

(2) (a) Carlucci, L.; Ciani, G.; Proserpio, D. M. *Coord. Chem. Rev.* **2003**, *246*, 247−289. (b) Zhang, Z.; Liu, J.; Li, Y.; Yao, S.; Wang, E.; Wang, X. *J. Solid State Chem.* **2010**, *183*, 228−233. (c) Shyu, E.; Supkowski, R. M.; LaDuca, R. L. *Inorg. Chem.* **2009**, *48*, 2723−2725.

(3) (a) Long, D. L.; Blake, A. J.; Champness, N. R.; Wilson, C.; Schröder, M. *Angew. Chem., Int. Ed.* **2001**, *40*, 2443−2447. (b) Long, D. L.; Hill, R. J.; Blake, A. L.; Champness, N. R.; Hubberstey, P.; Proserpio, D. M.; Wilson, C.; Schröder, M. *Angew. Chem., Int. Ed.* **2004**, *43*, 1851−1854. (c) Chun, H.; Kim, D.; Dybtsev, D. N.; Kim, K. *Angew. Chem., Int. Ed.* **2004**, *43*, 971−974.

(4) (a) Reineke, T. M.; Eddaoudi, M.; Moler, D. *J. Am. Chem. Soc.* **2000**, *122*, 4843−4844. (b) Lee, E.; Heo, J.; Kim, K. *Angew. Chem., Int. Ed.* **2000**, *39*, 2699−2701. (c) Cui, Y.; Ngo, H. L.; White, P. S.; Lin, W.-B. *Chem. Commun.* **2002**, 1666−1667. (d) Chen, L.; Jiang, F.; Lin, Z.; Zhou, Y.; Yue, C.; Hong, M. *J. Am. Chem. Soc.* **2005**, *127*, 8588−8589.

(5) (a) Jia, J.; Lin, X.; Wilson, C.; Blake, A. J.; Champness, N. R.; Hubberstey, P.; Walker, G.; Cussen, E. J.; Schröder, M. *Chem. Commun.* **2007**, 840−842. (b) Zhang, X.-M.; Fang, R.-Q.; Wu, H.-S. *J. Am. Chem. Soc.* **2005**, *127*, 7670−7671. (c) Li, D.; Wu, T.; Zhou, X.-P.; Zhou, R.; Huang, X.-C. *Angew. Chem., Int. Ed.* **2005**, *44*, 4175−4178.

(6) (a) Qu, X.; Xu, L.; Gao, G.; Li, F.; Yang, Y. *Inorg. Chem.* **2007**, *46*, 4775−4777. (b) Qi, Y.-F.; Lv, C.-P.; Wang, E.-B.; Lia, J.; Somg, X.-L. *Inorg. Chem. Commun.* **2010**, *13*, 384−387.

(7) Lee, J.; Farha, O. K.; Roberts, J.; Scheidt, K. A.; Nguyen, S. T.; Hupp, J. T. *Chem. Soc. Rev.* **2009**, *28*, 1450−1459.

(8) Rowsell, J. L.; Yaghi, O. M. *Angew. Chem., Int. Ed.* **2005**, *44*, 4670−4679.

(9) Fang, Q.-R.; Zhu, G.-S.; Ji, Y.-Y.; Ye, J.-W.; Xue, M.; Yang, H.; Wang, Y.; Qiu, S.-L. *Angew. Chem., Int. Ed.* **2007**, *46*, 6638−6642.

(10) Li, J.-R.; Kuppler, R. J.; Zhou, H.-C. *Chem. Soc. Rev.* **2009**, *38*, 1477−1504.

(11) Rao, C. N. R.; Cheetham, A. K.; Thirumurugan, A. *J. Phys: Condens. Matter* **2008**, *20*, 083202.

(12) Férey, G. *Chem. Soc. Rev.* **2008**, *37*, 191−214.

(13) Chernova, N. A.; Roppolo, M.; Dillonb, A. C.; Whittingham, M. S. *J. Mater. Chem.* **2009**, *19*, 2526−2552.

(14) Lin, H.; Maggard, P. A. *Inorg. Chem.* **2008**, *47*, 8044−8052.
(15) Zavalij, P. Y.; Whittingham, M. S. *Acta Crystallogr.* **1999**, *B55*, 627−663.
(16) Hargman, J.; Hargman, D.; Zubieta, J. *Angew. Chem., Int. Ed.* **1999**, *38*, 2638−2803.
(17) Blatov, V. A.; Carlucci, L.; Ciani, G.; Proserpio, D. M. *CrystEngComm* **2004**, *6*, 378−395.
(18) Bouhedja, L.; Steunou, M.; Maquet, J.; Livaje, J. *J. Solid State Chem.* **2001**, *162*, 315−321.
(19) (a) Larrea, E. S.; Mesa, J. L.; Pizarro, J. L.; Arriortua, M. I.; Rojo, T. *J. Solid State Chem.* **2007**, *180*, 1149−1157. (b) Larrea, E. S.; Mesa, J. L.; Pizarro, J. L.; Rodríguez-Fernández, J.; Arriortua, M. I.; Rojo, T. *Eur. J. Inorg. Chem.* **2009**, *24*, 3607−3612. (c) Larrea, E. S.; Mesa, J. L.; Arriortua, M. I. *Mater. Res. Bull.* **2011**, *46*, 845−849.
(20) Fernández de Luis, R.; Urtiaga, M. K.; Mesa, J. L.; Rojo, T.; Arriortua, M. I. *J. Alloys Compd.* **2008**, *480*, 54−56.
(21) (a) Goodwin, A. L.; Kepert, C. J. *Phys. Rev.* **2005**, *B71*, 140301(1)−140301(4). (b) Goodwin, A. L.; Calleja, M.; Conterio, M. J.; Dove, M. T.; Evans, J. S. O.; Keen, D. A.; Peters, L.; Tucker, M. G. *Science* **2008**, *319*, 794−797. (c) Korčok, J. L.; Matz, M. J.; Leznoff, D. B. *J. Am. Chem. Soc.* **2009**, *131*, 4866−4871.
(22) (a) Dubbleldam, D.; Walton, K. S.; Ellis, D. E.; Snurr, R. *Angew. Chem., Int. Ed.* **2007**, *46*, 4496−4499. (b) Peterson, V. K.; Kearley, G. J.; Wu, Y.; Ramírez-Cuesta, A. J.; Kemner, E.; Kepert, C. J. *Angew. Chem., Int. Ed.* **2010**, *49*, 585−588.
(23) (a) Chen, C. L.; Goford, A. M.; Smith, M. D.; Su, C. Y.; zur Loye, H. C. *Angew. Chem., Int. Ed.* **2005**, *44*, 6673−6677. (b) Haisheng, L.; Maggard, P. A. *Inorg. Chem.* **2008**, *47*, 8044−8052. (c) Larrea, E. S.; Pizarro, J. L.; Mesa, J. L.; Rodríguez-Fernández, J.; Arriortua, M. I.; Rojo, T. *Eur. J. Inorg. Chem.* **2009**, *34*, 3607−3612.
(24) Fernández de Luis, R.; Mesa, J. L.; Urtiaga, M. K.; Lezama, L.; Arriortua, M. I.; Rojo, T. *New. J. Chem.* **2008**, *32*, 1582−1589.
(25) Fernández de Luis, R.; Mesa, J. L.; Urtiaga, M. K.; Rojo, T.; Arriortua, M. I. *Eur. J. Inorg. Chem.* **2009**, 4786−4794.
(26) Yingua, W. *J. Appl. Crystallogr.* **1987**, *20*, 258−259.
(27) Altomare, A.; Cascarano, G.; Giacovazzo, C.; Guagliardi, A. *J. Appl. Crystallogr.* **1993**, *26*, 343−350.
(28) Sheldrick, G. M. *SHELX97, Programs for Crystal Structure Analysis*; Institüt für Anorganische Chemie, Universität Göttingen: Göttingen, Germany, 1998.
(29) Fernández de Luis, R.; Urtiaga, M. K.; Mesa, J. L.; Aguayo, A. T.; Rojo, T.; Arriortua, M. I. *CrystEngComm* **2010**, *12*, 1880−1886.
(30) (a) Blatov, V. A.; Shevchenko, A. P.; Serezhkin, V. N. *Acta Crystallogr., Sect. A: Found. Crystallogr.* **1995**, *51*, 909−916. (b) Baburin, I. A.; Blatov, V. A. *Acta Crystallogr., Sect. B: Struct. Sci.* **2004**, *60*, 447−452.
(31) (a) Lever, A. B. P. *Inorganic Electronic Spectroscopy*; Elservier Science: Amsterdam, The Netherlands, 1984. (b) Sugano, T. Y. *J. Phys. Soc. Jpn.* **1954**, *9*, 753−766.
(32) (a) Carlin, R. L. *Magnetochemistry*; Springer-Verlag: Berlin, Germany, 1986. (b) Nanda, K. K.; Thompson, L. K.; Bridson, J. N.; Nag, J. *Chem. Soc., Chem. Commun.* **1994**, 1337.
(33) (a) AllenF. H.KennardO.Chem. Des. Autom. News1993 ; update Aug. 2008, v. 5.29. Ordered and error free crystal structures containing the Bpa ligand with *R* values <0.05 were analyzed(b) Allen, F. H.; Motherwell, W. D. S. *Acta Crystallogr., Sect. B: Struct. Sci* **2002**, *58*, 407−422.